Comparing modeling predictions of aluminum edge dislocations: semidiscrete variational Peierls-Nabarro versus atomistics

Lucas M. Hale

Materials Science and Engineering Division, National Institute of Standards and Technology, Gaithersburg, MD 20899 USA

Corresponding e-mail:
lucas.hale@nist.gov

Abstract

Multiple computational methods for modeling dislocations are implemented within a high-throughput calculation framework allowing for rigorous investigations comparing the methodologies. Focusing on aluminum edge dislocations, twenty-one classical aluminum interatomic potentials are used to directly model dislocation core structures using molecular dynamics, as well as provide input data for solving the semidiscrete variational Peierls-Nabarro dislocation model. The predicted dislocation core spreading obtained from both computational methods show similar trends across the potentials. Additionally, tests are done to rigorously determine if a recent correction to the Peierls-Nabarro model results in better agreement with the atomistic calculations.

Introduction

Dislocations in crystalline materials typically dominate yield and hardening mechanisms. Accurate computational models of dislocation core structures provide insight into the nature of the dislocation, and can lead to the development of improved physically-based yield models. While direct atomistic simulations of dislocations for simple materials is commonplace, directly modeling dislocation core structures in complex materials can prove challenging. With classical atomistic potentials, there is always uncertainty in properties and interactions around defects, especially in multi-component systems. Quantum-based calculations, e.g. density functional theory (DFT), offer a more robust description of defects, but they may be too expensive for dislocations with wide cores.

The semidiscrete variational Peierls-Nabarro (SDVPN) model [1-3] can be used to predict the spreading of a dislocation's core. In the Peierls-Nabarro model, the dislocation is represented as a continuum spread of infinitesimal Volterra dislocations. The SDVPN model offers a numerical approximation in which the displacement caused by the dislocation is evaluated at equally spaced positions and assumed constant between those positions. Typically, positions match the spacings of atomic columns along the slip plane, giving the spreading an apparent discreteness corresponding to actual atomic discreteness. The advantage of the SDVPN model is that it can provide a prediction for the dislocation spreading based only on a generalized stacking fault energy map, i.e. gamma surface, and elastic constants, both of which can be obtained using DFT, even for complex materials.

There have been proposed corrections to improve the SDVPN model. Miller et. al. [4] used a non-local Kernel that linearly added interactions between increasingly separated pairs of model evaluation coordinates. Wang [5] considered the surface effect along the slip plane to derive a correction term with coefficients related to phonon velocities and crystal geometries. This surface effect correction has been used to model dislocations in a wide range of materials using DFT data [6-10]. Recently, Liu, et. al. [11-13] showed that either correction can be numerically fit to atomistic results.

The computational methods associated with direct atomistic modeling of dislocations and solving the SDVPN model are implemented in the openly available iprPy high-throughput calculation framework (https://github.com/usnistgov/iprPy). The high-throughput framework allows calculations to be performed across a wide range of input parameters, such as composition, dislocation type, interatomic potential, and calculation size. This setup also allows direct comparison of the results from the different calculation methods to help validate and verify that the methodologies are sound and meaningful.

This paper investigates the impact that the surface effect correction has on SDVPN predictions of aluminum $\frac{a}{2}\langle 110 \rangle$ edge dislocations. The choice of aluminum edge dislocation is practical as direct atomistic representations can be obtained with classical potentials, and the potentials are known to give a wide range of stacking fault behaviors [14]. Using twenty-one classical interatomic potentials, the correction term is evaluated based on how it improves the predicted dislocation structure relative to atomistic results, and the transferability of the correction across the different potentials.

Atomistic simulations

Atomistic simulations are performed with the LAMMPS software [15] using classical interatomic potentials for aluminum obtained from the Interatomic Potential Repository website (http://www.ctcms.nist.gov/potentials). For each potential, the face-centered cubic (fcc) lattice constants are evaluated by performing an energy minimization that simultaneously relaxes the box dimensions to zero pressure. The minimization procedure is repeated until the lattice constants are observed to converge. Elastic constants are estimated by applying small strains of 10^{-8} to the relaxed system and measuring the resulting change in the system's total virial stresses.

2D gamma surfaces for the (111) fcc crystallographic plane are evaluated by constructing an atomic system with crystallographic vector dimensions of $5[1\bar{1}0]\times 5[11\bar{2}]\times 10[111]$. The x- and y-boundaries are kept periodic, while the z-boundary is non-periodic. A (111) plane at the center of the z-direction is identified, and all atoms above that plane are shifted by a fractional combination of two shift vectors, $s_i = \frac{1}{2}[1\bar{1}0]$ and $t_i = \frac{1}{2}[11\bar{2}]$. A total grid of 51×51 points is evaluated, with each point having a shift of $Xs_i/50 + Yt_i/50$, where X and Y are integers. At each shift, the system's total energy is computed after allowing atomic relaxations in the z-direction. The fault energy at each point is taken relative to the zero shift (i.e. $X = Y = 0$) point, and divided by the area of the slip plane.

The Stroh method is used to solve the Eshelby anisotropic dislocation model based on the proper crystal orientation, and the lattice and elastic constants for each potential. Dislocation monopole systems are constructed by applying the Stroh solution's displacements to an initially perfect fcc system with crystallographic vector dimensions of $98[10\bar{1}]\times 80[111]\times 2[1\bar{2}1]$, producing a dislocation along the system's z-axis. The system is divided into two regions: an active cylindrical region centered on the z-axis, and an inactive region at the x- and y-boundaries. The radius of the active region is around $66a \approx 265$ Å, which insures the inactive region is at least $3a$ thick everywhere. The positions of the atoms in the active region are relaxed through a short thermal anneal followed by an energy minimization, while the atoms in the inactive region are held fixed at the elastic solution. Size-dependent tests showed halving or doubling the system dimensions to have negligible effects on the dislocation structure.

Twenty-one potentials with aluminum elemental interactions [16-33] were identified that predict a stable face-centered cubic aluminum structure, and a relaxed dislocation structure consisting of two partial dislocations. Further discussion on the potentials can be found in the supplementary material (refer to online supplementary material).

Semidiscrete variational Peierls-Nabarro model

The SDVPN model allows for the core spreading of a dislocation to be solved by identifying the planar disregistry, i.e. relative displacement above and below the slip plane, that minimizes the dislocation's energy. The dislocation line is taken along the z-axis, and the slip

plane corresponds to the $y = 0$ plane. The dislocation's disregistry vector, δ_i, is evaluated at N positions along the x-axis, all equally spaced by Δx.

The total energy of the dislocation is expressed as a function of the disregistry at all x evaluation positions, and consists of a sum of energy terms

$$U_{dislocation} = U_{misfit} + U_{elastic} + U_{stress} + U_{surface}. \quad (1)$$

Only the zero-stress configurations are investigated here, thus the stress energy term is not used. The disregistry is initially taken as an arctan function, and has fixed endpoints of $\delta_i\left(x^{(1)}\right) = 0$ and $\delta_i\left(x^{(N)}\right) = b_i$. The remaining disregistry values are updated to minimize Eq. (1) using Powell's minimization method [34].

The misfit energy is taken as

$$U_{misfit} = \sum_{\alpha=1}^{N} \gamma\left(\delta_i\left(x^{(\alpha)}\right)\right)\Delta x, \quad (2)$$

where γ is the generalized stacking fault energy corresponding to a stacking fault given by the disregistry at a position $x^{(\alpha)}$. Only 2D gamma surfaces are considered, thus the disregistry perpendicular to the slip plane, δ_2, is taken as 0 for all $x^{(\alpha)}$. Generalized stacking fault energies between the measured atomistic values are interpolated using a multiquadric radial basis function.

The short-range configuration-dependent elastic energy of the dislocation is calculated as

$$U_{elastic} = \frac{1}{4\pi} \sum_{\alpha=1}^{N} \sum_{\beta=1}^{N} \chi(\alpha,\beta) K_{ij} \rho_i\left(x^{(\alpha)}\right) \rho_j\left(x^{(\beta)}\right), \quad (3)$$

where K_{ij} is the energy coefficient tensor, ρ_i is the dislocation density given by $\rho_i\left(x^{(\alpha)}\right) = \left(\delta_i\left(x^{(\alpha)}\right) - \delta_i\left(x^{(\alpha-1)}\right)\right)/(\Delta x)$, and $\chi(\alpha,\beta)$ is a multiplicative factor. Anisotropic values of K_{ij} are obtained from the Stroh method. Here, K_{ij} is defined such that in the isotropic case $K_{11} = K_{22} = \mu/(1-\nu)$ and $K_{33} = \mu$, where μ and ν are the shear modulus and Poisson's ratio, respectively. The χ factor is calculated for each pair of α, β indices as

$$\chi(\alpha,\beta) = (3/2)\Delta x^2 + \psi(\alpha-1,\beta-1) + \psi(\alpha,\beta) - \psi(\alpha,\beta-1) - \psi(\beta,\alpha-1), \quad (4a)$$

$$\psi(\alpha,\beta) = (1/2)(\alpha-\beta)^2 \Delta x^2 \ln\left(|\alpha-\beta|\Delta x\right). \quad (4b)$$

The expressions for χ and ψ are simplified from the original forms in [1] by assuming a constant Δx.

The final term, the surface effect energy is taken as

$$U_{surface} = \frac{1}{4}\sum_{\alpha=1}^{N} B_i \left(\frac{\delta_i\left(x^{(\alpha+1)}\right) - \delta_i\left(x^{(\alpha-1)}\right)}{2\Delta x} \right)^2 \Delta x \,. \tag{5}$$

This corresponds to the correction term derived by Wang [5] for dislocations on slip planes with rotational symmetry, and uses the discrete summation formula used by Liu [11]. The B_i constants can be analytically calculated as

$$B_1 = \frac{3\Omega}{4\sigma}\left(C_l - C_{tv}\tan^2\theta\cos^2\phi\right), \tag{6a}$$

$$B_3 = \frac{3\Omega}{4\sigma}\left(C_{th} - C_{tv}\tan^2\theta\sin^2\phi\right), \tag{6b}$$

where Ω is the volume density of the crystal's unit cell, σ is the area density along the glide plane, θ and ϕ are crystal-dependent orientation angles relating to relative neighbor atom vectors, and C_l, C_{th}, and C_{tv} are the effective elastic constants associated with longitudinal and transverse phonons. For a (111) fcc slip plane, $\tan\theta = 1/\sqrt{2}$, $\phi = \pi/6$, and Ω/σ reduces to the (111) interplanar spacing. For phonons propagating along a close-packed <110> direction, the effective elastic constants are

$$C_l = \left(C_{11} + C_{12} + 2C_{44}\right)/2\,, \tag{7a}$$

$$C_{th} = \left(C_{11} - C_{12}\right)/2\,, \tag{7b}$$

$$C_{tv} = C_{44}. \tag{7c}$$

The quality of the SDVPN models, with and without the surface correction, is evaluated by comparing the predicted disregistry from the model, $\delta_i^{(PN)}$, to the measured disregistry from the atomistic calculations, $\delta_i^{(MD)}$. The discrepancy between the two methods is quantitatively evaluated as the sum squared error between $\delta_i^{(PN)}$ and $\delta_i^{(MD)}$

$$\kappa^2 = \sum_{\alpha}\left[\delta_i^{(MD)}\left(x^{(\alpha)}\right) - \delta_i^{(PN)}\left(x^{(\alpha)}\right)\right]^2 . \tag{8}$$

This κ^2 discrepancy is also used to find optimized SDVPN models based on Eqs. (1-5) for each potential. Following the work of Liu [11], the model is simplified by setting the two B_i components to be equal, i.e. $B_1 = B_3 = B$, and then finding the B value that minimizes κ^2.

Results

Initial tests with the SDVPN model showed that *x* values corresponding to $\Delta x = a\sqrt{2}/4$ and $N = 100$ or $N = 101$ total points were sufficient to capture the dislocation's shape and spreading for all potentials evaluated. Calculations are performed with two values of N as having an even versus an odd number of points results in the *x* positions differing by $\Delta x/2$. Figure 1 shows that the two N values produce disregistry profiles that overlay each other, but are evaluated at different positions. While this behavior has little impact on the predicted dislocation shape, it is important when evaluating κ^2 between SDVPN solutions and the atomistic results.

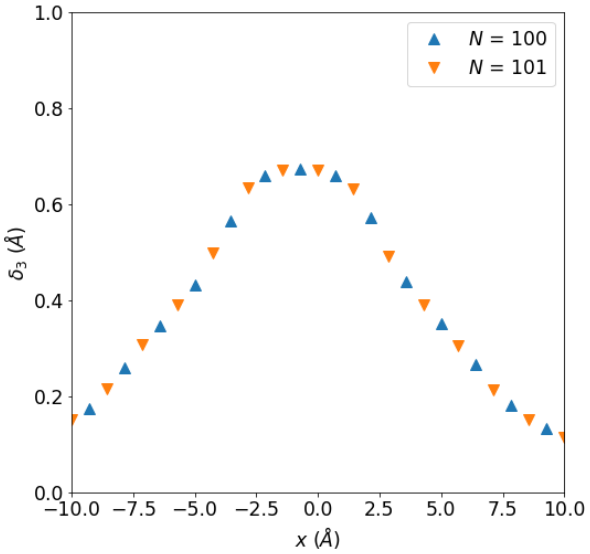

Figure 1: Shifting the evaluated x-coordinates by Δx/2 produces disregistry trend that overlay each other despite different positions being evaluated.

The analytical B_i constants are calculated using Eqs. 6 and 7 and the lattice and elastic constants computed for each potential. While values do vary across the potentials, most have

similar elastic constants ($C_l \approx 120$ GPa, $C_{th} \approx 25$ GPa, and $C_{tv} \approx 30$ GPa) resulting in B_i values around $B_1 \approx 19$ Pa*m and $B_3 \approx 4$ Pa*m.

The fitted B constants are also obtained for every potential. The atomistic disregistry profile is shifted to align with the uncorrected SDVPN solution. Shifting is necessary as the partial dislocations are not always equidistant from the center of the atomistic system following the thermal anneal. The shift is observed to be a small, random adjustment that varies from potential to potential, even among potentials with the same aluminum interaction model. Each evaluation in the optimization process solves the SDVPN model for a value of B starting with the uncorrected SDVPN disregistry solution as the initial guess. Across the potentials, the fitted B values are found to range from 5 to 18 Pa*m, placing the fitted values between the analytical B_1 and B_3 constants. For potentials with the same elemental interactions, the fitted B values were observed to vary by as much as 1.5 Pa*m. This variation is primarily attributed to differences in alignment; only the $N = 101$ solution and a single shift was tested per potential.

Figure 2 shows disregistry profiles as computed both with the SDVPN model (lines) and atomistics (shapes) for three potentials. The potentials shown were selected to highlight the range of predictions observed across the potentials investigated. Disregistry profiles for the remaining potentials fall between the 2015--Pascuet-M-I--Al and 2002--Mishin-Y--Ni-Al curves. The difference in disregistries across the potentials is primarily dependent on the intrinsic stacking fault energy for that potential (refer to online supplementary material).

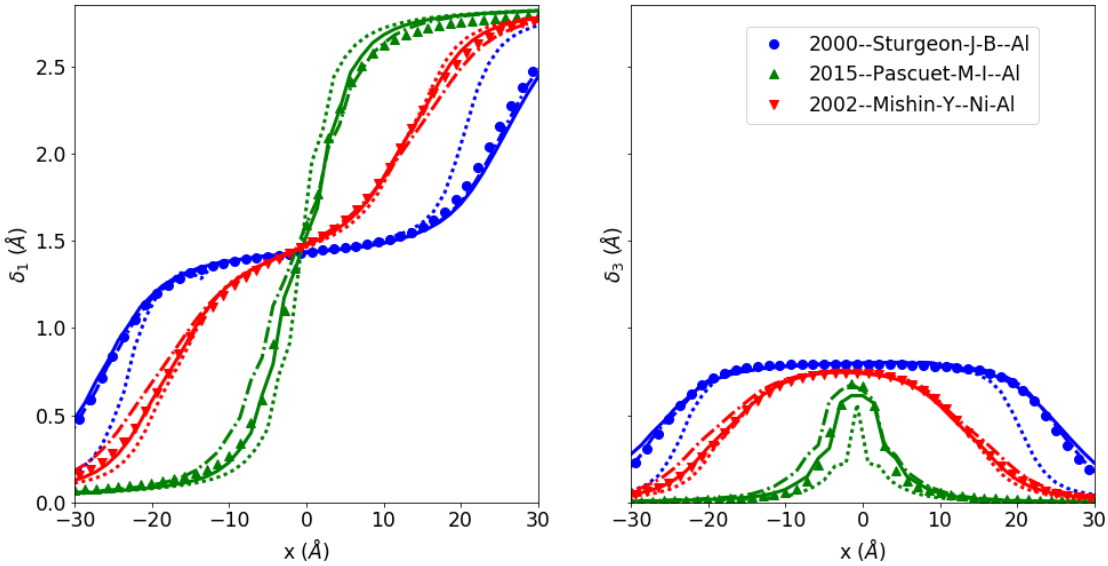

Figure 2: Disregistry profiles for three different interatomic potentials. The atomistic data is given by shapes, the uncorrected SDVPN model by dotted lines, the corrected model with analytical B_i values by dash-dotted lines, and the corrected model with fitted B values by solid lines.

Figure 2 also provides a qualitative comparison of how well the SDVPN model agrees with the atomistic results. The original uncorrected SDVPN model (dotted lines) gives the rough shape of the atomistic disregistry profile (shapes), but noticeable disagreements can be seen, especially in the regions with large changes in the disregistry with respect to *x*. Adding the surface energy correction with either the analytically calculated B_i constants (dash-dotted lines) or the fitted B constant (solid lines) qualitatively produces better agreements with the atomistic data.

Figure 3a plots κ^2 values for all the potentials. For the uncorrected and the analytical values, the smallest κ^2 between the $N=100$ and $N=101$ solutions are used. The SDVPN model with the surface correction consistently has a comparable or smaller κ^2 than the model without the correction. For the uncorrected model, the mean and standard deviation in κ^2 across all potentials are 0.67 Å^2 and 0.29 Å^2, respectively. Applying the correction with the analytical

B_i values improves these values to 0.15 Å^2 and 0.12 Å^2, respectively, and the fitted B values improves them to 0.078 Å^2 and 0.045 Å^2, respectively.

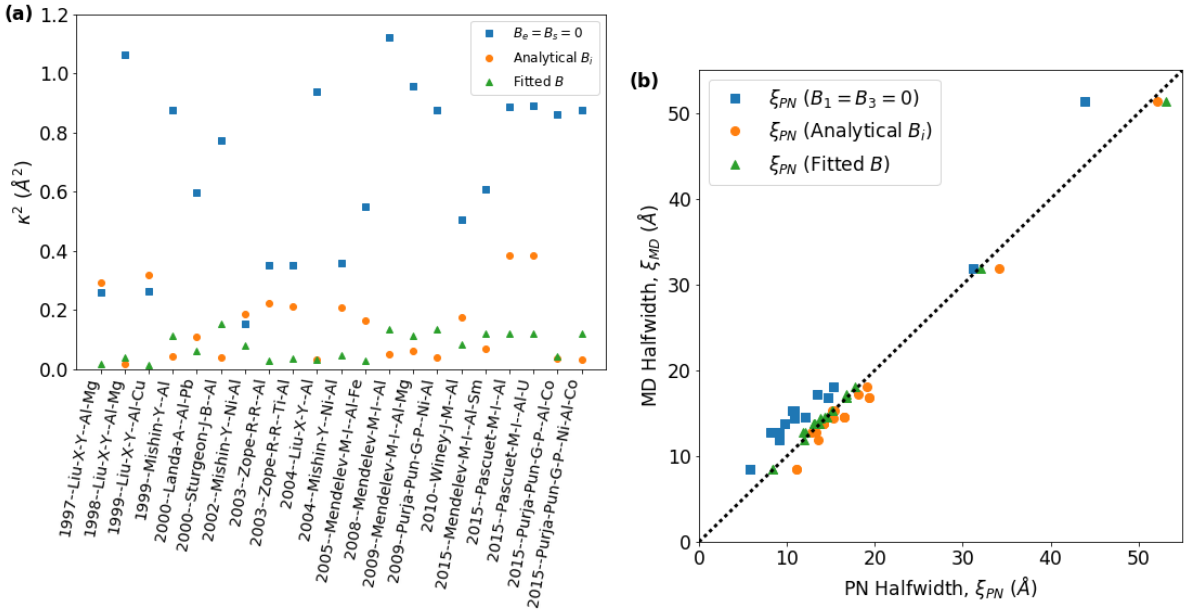

Figure 3: Quantitative evaluations of the agreement in predicted disregistry between the SDVPN models and the atomistic results. (a) The κ^2 discrepancy for each potential. (b) Dislocation halfwidth values.

An alternate metric for evaluating the agreement between the SDVPN models and atomistic results is the dislocation's halfwidth, ξ. The halfwidth was estimated by linearly interpolating the x-coordinates where $\delta_1(x) = |b_i|/4$ and $\delta_1(x) = 3|b_i|/4$. Figure 3b plots ξ_{PN} for the different model options versus ξ_{MD} revealing varying levels of agreement. The uncorrected model under-predicts the atomistic halfwidth by an average of 3.4 Å, while the model with the analytical B_i values slightly over-predicts by an average of 1.2 Å, and the model with the fitted B constants is off by an average of only 0.2 Å.

Practically, the results suggest that the analytical B_i values are more transferable across potentials than the fitted B values. For the same element, variations in the analytical values are small, and can be easily tuned to a specific potential using its elastic constants. In contrast, the fitted values are observed to strongly vary across potentials. Obtaining an optimum B value for a potential requires that a full atomistic representation be possible and available. Taken together,

this indicates that the analytical version is more applicable to more expensive and robust atomistic potentials, such as DFT, where direct atomistic representations may not be easily obtainable.

Summary and Conclusions

Methods for predicting dislocation structures using either direct atomistic simulations or the SDVPN model are implemented in an open source, high-throughput computational framework. Implementing the calculations into the framework allows for comprehensive investigations to be performed across a range of input parameters. Here, aluminum edge dislocations are evaluated using twenty-one classical interatomic potentials and for the SDVPN model with and without a recent correction term.

Evaluating the same dislocation structure with multiple classical interatomic potentials demonstrates the sensitivity of the results to the choice of potential, and reveals trends across the predictions. Comparisons of dislocation disregistry predictions between the various methods show that including the slip plane surface energy correction in the SDVPN model consistently improves the model. Averaging evaluation metrics across the potentials also provides a rough estimate of the error associated with the SDVPN methods themselves.

Further work is needed to investigate other options of the SDVPN model and how universal the results shown here are across compositions and dislocation types. Expanding the fitting procedure to independently solve both B_i constants should be explored to determine if it offers constants that are more transferable across potentials. Using full 3D gamma surfaces may be important for certain potentials or dislocation structures. Investigating the influence of the surface correction on other dislocation types, especially asymmetric dislocations, is needed as the term's formulation is based on symmetry assumptions.

References

[1] V.V. Bulatov and E. Kaxiras, *Phys. Rev. Lett.*, 78, 4221, (1997).

[2] G. Lu, N. Kioussis, V.V. Bulatov, and E. Kaxiras, *Phys. Rev. B*, 62, 3099 (2000).

[3] G. Lu, N. Kioussis, V.V. Bulatov, and E. Kaxiras, *Philos. Mag. Lett.*, 80, 675 (2000).

[4] R. Miller, R. Phillips, G. Beltz, and M. Ortiz, *J. Mech. Phys. Solids*, 46, 1845 (1998).

[5] S.F. Wang, *J. Phys. A: Math. Theor*. 42, 025208 (2009).

[6] R. Wang, S.F. Wang, X.Z. Wu, and Q.Y. Wei, *Phys. Scr.*, 81, 065601 (2010).

[7] X.Z. Wu, S.F. Wang, and R.P. Liu, *Acta Mech. Sin.* 26, 425 (2010).

[8] R. Wang, S.F. Wang, and X.Z. Wu, *Phys. Scr.*, 83, 045604 (2011).

[9] Y.Z. Jiang, R. Wang, and S.F. Wang, *Philos. Mag.*, 96, 2829 (2016).

[10] S.R. Li, X.Z. Wu, T. Zhang, Y.X. Tian, Z.X. Yan, and H.Z. Zhu, *Phys. Chem. Miner.*, 43, 563 (2016).

[11] G.S. Liu, X. Cheng, J. Wang, K.G. Chen, and Y. Shen, *Scr. Mater.*, 120, 94 (2016).

[12] G.S. Liu, X. Cheng, J. Wang, K.G. Chen, and Y. Shen, *Comput. Mater. Sci.*, 131, 69 (2017).

[13] G.S. Liu, X. Cheng, J. Wang, K.G. Chen, and Y. Shen, *Sci. Rep.* 7, 43785 (2017).

[14] Z.T. Trautt, F. Tavazza, and C.A. Becker, *Modell. Simul. Mater. Sci. Eng*., 23, 074009 (2015).

[15] S. Plimpton, *J. Comp. Phys*., 117, 1 (1995).

[16] X.Y. Liu, P.P. Ohotnicky, J.B. Adams, C.L. Rohrer, and R.W. Hyland, *Surf. Sci.*, 373, 357 (1997).

[17] X.Y. Liu, and J.B. Adams, *Acta Mater.*, 46, 3467 (1998).

[18] X.Y. Liu, C.L. Liu, and L.J. Borucki, *Acta Mater.*, 47, 3227 (1999).

[19] Y. Mishin, D. Farkas, M.J. Mehl, and D.A. Papaconstantopoulos, *Phys. Rev. B*, 59, 3393 (1999).

[20] A. Landa, P. Wynblatt, D.J. Siegel, J.B. Adams, O.N. Mryasov, and X.Y. Liu, *Acta Mater.*, 48, 3621 (2000).

[21] J.B. Sturgeon, and B.B. Laird, *Phys. Rev. B*, 62, 14720 (2000).

[22] Y. Mishin, M.J. Mehl, and D.A. Papaconstantopoulos, *Phys. Rev. B*, 65, 224114 (2002).

[23] R.R. Zope, and Y. Mishin, *Phys. Rev. B*, 68, 024102 (2003).

[24] X.Y. Liu, F. Ercolessi, and J.B. Adams, *Modell. Simul. Mater. Sci. Eng*., 12, 665 (2004).

[25] Y. Mishin, *Acta Mater.*, 52, 1451 (2004).

[26] M.I. Mendelev, D.J. Srolovitz, G.J. Ackland, and S. Han, *J. Mater. Res.*, 20, 208 (2005).

[27] M.I. Mendelev, M.J. Kramer, C.A. Becker, and M. Asta, *Philos. Mag.*, 88, 1723 (2008).

[28] M.I. Mendelev, M. Asta, M.J. Rahman, and J.J. Hoyt, *Philos. Mag.*, 89, 3269 (2009).

[29] G.P.P. Pun, and Y. Mishin, *Philos. Mag.*, 89, 3245 (2009).

[30] J.M. Winey, K. Alison, and Y.M. Gupta, *Modell. Simul. Mater. Sci. Eng*., 17, 055004 (2009).

[31] J.M. Winey, K. Alison, and Y.M. Gupta, *Modell. Simul. Mater. Sci. Eng*., 18, 029801 (2010).
[32] M.I. Pascuet, and J.R. Fernandez, *J. Nucl. Mater.*, 467, 229 (2015).
[33] G.P. Purja Pun, V. Yamakov, and Y. Mishin, *Modell. Simul. Mater. Sci. Eng*., 23, 065006 (2015).
[34] M.J.D. Powell, *Comput. J.* 7, 155 (1964).